



HAL
open science

Flow Activation Energy Estimation by Thermo-Rheological Method

Qiao Lin, Nadine Allanic, Manuel Girault, Pierre Mousseau

► **To cite this version:**

Qiao Lin, Nadine Allanic, Manuel Girault, Pierre Mousseau. Flow Activation Energy Estimation by Thermo-Rheological Method. *Macromolecular Reaction Engineering*, 2023, 17 (5), pp.2300019. 10.1002/mren.202300019 . hal-04294485

HAL Id: hal-04294485

<https://hal.science/hal-04294485>

Submitted on 20 Nov 2023

HAL is a multi-disciplinary open access archive for the deposit and dissemination of scientific research documents, whether they are published or not. The documents may come from teaching and research institutions in France or abroad, or from public or private research centers.

L'archive ouverte pluridisciplinaire **HAL**, est destinée au dépôt et à la diffusion de documents scientifiques de niveau recherche, publiés ou non, émanant des établissements d'enseignement et de recherche français ou étrangers, des laboratoires publics ou privés.

Flow Activation Energy Estimation by Thermo-Rheological Method

Qiao Lin, Nadine Allanic,* Manuel Girault, and Pierre Mousseau

Polymer and many other flows exhibit non-Newtonian rheological behavior. For some materials, the thermal dependence of viscosity is also essential to be established. It can be described by considering an activation energy, estimated by using the viscosity measurements at different temperatures. Nevertheless, the test temperatures must be reliable and accurate. An annular measuring device (TRAC: Thermo-Rheo Annular Cell) is previously proposed for highly robust temperature measurement and viscosity identification by inverse method, which exploits the viscous dissipation in the flow. This work explains how critical viscosity points, identified thanks to the TRAC, can be used to estimate the activation energy with different approaches involving the principle of time-temperature superposition. Thanks to the thermal characteristics of the annular flow, the thermal dependence of viscosity can also be estimated from direct temperature measurements to perform fast analysis, without using inverse method.

1. Introduction

In a polymer production process, the mass transfer of the material occurs at high temperature. One of the key properties of mass transfer, viscosity, can strongly depend on temperature.^[1] The Eyring theory can be used to model the temperature-dependent behavior of the viscosity.^[2] The enthalpy change related to molecular motion leads to an Arrhenius type equation.^[3] This approach gives a physical meaning to the activation energy term in the Arrhenius law when the latter is employed for viscosity modeling.

To estimate the activation energy, the viscosity should be measured precisely at different temperatures. Different viscosity measurement techniques exist, such as capillary method.^[4] or dynamic method.^[5] However, in most viscosity measuring devices, temperature measurements are effectuated by wall-mounted

thermocouples, which can be heavily dominated by the temperature of the solid parts.^[6]

An annular measuring device.^[7] (TRAC: Thermo-Rheo Annular Cell) is designed to improve the quality of temperature measurement of polymer flow. Thermocouples are installed on the central axis of the annular structure to measure the temperature, when polymer flows through the device in the axial direction (Figure 1, where $[T_{obs}]_i$ stands for the measurement of thermocouple i). The central axis surrounded by the axial polymer flow is thus isolated, to a certain extent, from external thermal disturbances coming in the radial direction (Figure 1). Besides, the presence of the central axis generates an extra viscous dissipation in the flow. The temperature variation due to the

viscous dissipation will be directly recorded by thermocouples on the central axis and used to identify the viscosity of the polymer. A critical viscosity point is found to be related to this temperature variation, under well-defined flow conditions.^[8,9] When the flow conditions, especially the flowrate, are changed, a different critical viscosity point can be obtained. Thanks to the TRAC, the viscosity can be identified with reliable temperature measurements.

The TRAC is designed to be used as an extended nozzle.^[7,9] During polymer injection molding production, the polymer melt from the screw-barrel will first pass through the instrumented annular structure and then into a mold.

In this paper, a numerical study is first conducted to demonstrate the possibility of using the viscous dissipation method.^[8,9] to analyze the thermal dependence of viscosity and to estimate the activation energy. The simulation results are discussed to develop different approaches for the activation energy estimation process with the TRAC.

The first approach is based on the power-law model of viscosity.^[10,11] with the Arrhenius law^[3] acting on the viscosity term. Analyses are performed to simplify the process for quick estimation applications with directly measured signals. The second approach is based on the principle of time-temperature superposition, involving at least three critical viscosity points identified by inverse method.

Then, an experiment is carried out to estimate the activation energy of a polystyrene melt flowing through the TRAC.^[7]

2. Setup of the Preliminary Numerical Study

The activation energy can be estimated from viscosities identified at different temperatures, that is, the thermal dependence

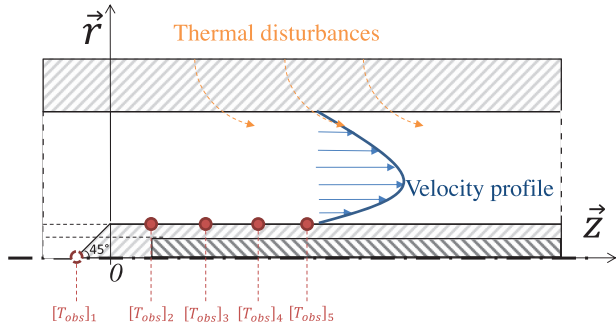


Figure 1. Annular flow scheme.

of viscosity. The analysis is performed under annular axial flow conditions to apply a new viscosity identification method, based on the viscous dissipation phenomenon.^[8,9]

2.1. Virtual Measurements

Virtual measurements are generated by a finite element model with « ANSYS POLYFLOW » software. The model is described in the previous study^[12] and it uses the power law (Equation (1)).^[10,11]

$$\eta = K\dot{\gamma}^{n-1} \quad (1)$$

with η the dynamic viscosity, $\dot{\gamma}$ the generalized shear rate, K the consistency factor and n the pseudo-plasticity index. One difference is that the Arrhenius law (Equation (2)).^[3] is added to the model to simulate the thermal dependence of viscosity,

$$\frac{\eta(T)}{\eta(T_0)} = \exp\left[\frac{E_a}{R_g}\left(\frac{1}{T} - \frac{1}{T_0}\right)\right] \quad (2)$$

where T is the absolute temperature, T_0 is a reference temperature in the absolute temperature scale, E_a is the activation energy and R_g is the perfect gas constant. The change in viscosity as a function of temperature is therefore written as Equation (3).

$$\frac{\partial\eta}{\partial T} = -\frac{E_a\eta}{R_g T^2} \quad (3)$$

We choose $E_a = 50 \text{ kJ}\cdot\text{mol}^{-1}$, $T_0 = 473.15 \text{ K}$, $K = 6585 \text{ Pa}\cdot\text{s}^n$ and $n = 0.412$ to simulate a polypropylene.^[1,13] For a material having an activation energy of $50 \text{ kJ}\cdot\text{mol}^{-1}$ at 473.15 K , $\Delta\eta/\eta \approx -0.027\Delta T$, that is to say that for 1° difference in temperature, the viscosity varies by 2.7%.

Two simulations of polymer melt flowing through the TRAC are carried out. The flowrate is $56.5 \text{ cm}^3 \text{ s}^{-1}$ for both simulations. In the first simulation (S_1), the inlet temperature, the set temperature and the initial temperature are at 473.15 K . In the second simulation (S_2), these temperatures are at 483.15 K . For each simulation, the initial time step is 0.001 s and the largest calculation time step is $<0.1 \text{ s}$. The initial time value is 0 s and the upper time limit is set to 2 s to simulate a two-second polymer injection.

The output of these simulations is the change in temperature over time (due to the viscous dissipation) measured by each

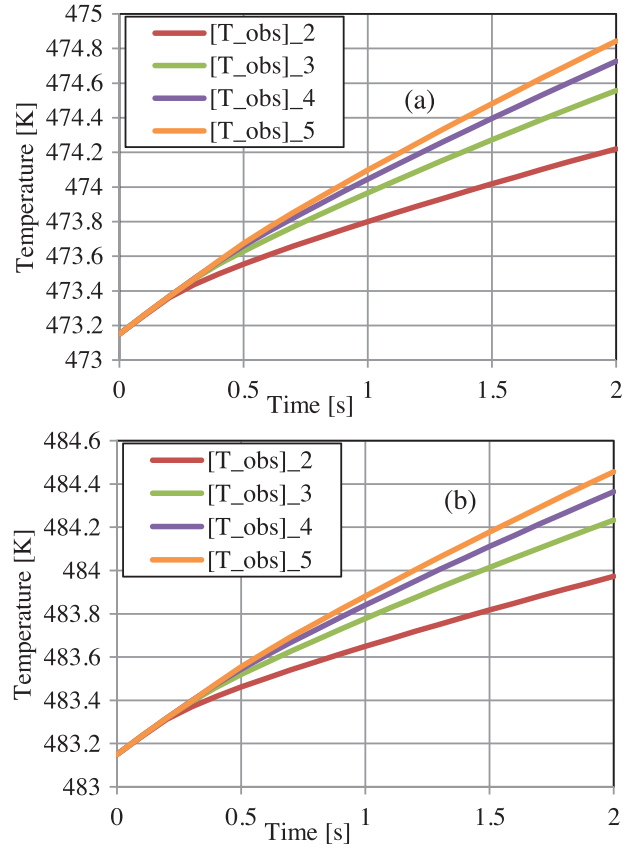


Figure 2. Virtual measurements with temperature conditions at a) 473.15 K and b) 483.15 K .

virtual thermocouple along the central axis (Figure 1). The positions of the virtual thermocouples are described in the previous study,^[12] which names the thermocouple measurements as $[T_{obs}]_i$. Virtual measurements $[T_{obs}]_i, i \in \{2; 5\}$ are presented in Figure 2. $[T_{obs}]_1$ (closest to the inlet) is at the tip of the conical shape of the central axis.^[12] and is not taken into account in this study, since it is also absent in the viscosity identification method,^[8] which will be described in the next section.

2.2. Viscosity Identification by Inverse Method

Temperature variations due to the viscous dissipation are used as information to identify a critical point (critical shear rate and critical viscosity: $(\dot{\gamma}_c, \eta_c)$).^[8,9] for each of the cases in Figure 2 (with temperature conditions at 473.15 K or 483.15 K). The identification is effectuated by inverse method, that is, the inverse method is executed twice, once with the data in Figure 2a and once with those in Figure 2b. Two critical points are obtained in total.

It's been observed that the critical shear rate $\dot{\gamma}_c$ varies slightly with the flow duration and greatly with the flowrate.^[8] Since the simulations are performed under the same flowrate for a duration of two seconds, $\dot{\gamma}_c$ remains the same. When the temperature of the flow is higher, the identified critical viscosity should be lower. Having two critical viscosity values for the same critical shear rate, the thermal dependence of viscosity can be determined, as well as the activation energy.

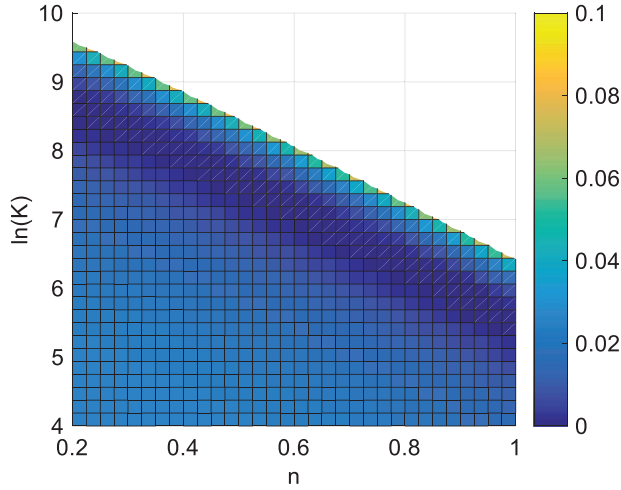


Figure 3. Example of the cost function's surface.^[8]

The reduced order model^[12] is chosen as the direct model in the inverse method. Different from the full order finite element model, the reduced order model employs the power law without thermal dependence. The input variables of the reduced order model are K , n and the flowrate. The output of the reduced order model is temperatures calculated at several different positions. We could have used another viscosity law in the reduced order model. However, when the temperature variations due to the viscous dissipation are sensitive to a critical viscosity point ($\dot{\gamma}_c, \eta_c$), the use of power law or other laws will lead us to the same critical point.

We use $T_{i,j}$, $i \in \{2; 5\}$ to represent the temperature calculated by the reduced order model at the position of thermocouple number i at recorded time number j . $[T_{obs}]_{i,j}$, $i \in \{2; 5\}$ is the virtual measurement obtained with the finite element model for thermocouple number i at recorded time number j . The cost function J_v of the inverse method can be written as Equation (4),

$$J_v = \frac{\sum_{j=1}^{N_t} \sum_{i=2}^{N_{Th}} (T_{i,j} - [T_{obs}]_{i,j})^2}{(N_{Th} - 1) N_t} \quad (4)$$

with N_{Th} the number of thermocouples, N_t the number of recorded instants. An example of the cost function's surface as a function of the power-law parameters (n , $\ln(K)$) is presented in Figure 3.

When using, for example, the data in Figure 2a as reference measurements $[T_{obs}]_{i,j}$, the surface of the cost function is close to the one in Figure 3. A nearly straight minimum valley can be observed instead of a unique minimum point.^[8] The valley can be defined as a linear relation (Equation (5)) between n and $\ln(K)$.

$$\ln(K) = -\ln(\dot{\gamma}_c) n + \ln(\eta_c) + \ln(\dot{\gamma}_c) \quad (5)$$

Equation (5) is in fact the power law (Equation (1)) on a natural logarithmic scale, representing different power-law curves passing through the same critical point ($\dot{\gamma}_c, \eta_c$). By knowing the equation of the minimum valley, we can identify the critical point ($\dot{\gamma}_c, \eta_c$).

In practice, we use second order line search to identify a K_1 value with a fixed n_1 value. We repeat the line search to identify a K_2 value with a different n_2 value. By injecting two sets of (n , $\ln(K)$) values for Equation (5), we can calculate the critical point ($\dot{\gamma}_c, \eta_c$) with Equations (6) et.

$$\dot{\gamma}_c = \exp\left(\frac{\ln(K_1) - \ln(K_2)}{n_2 - n_1}\right) \quad (6)$$

$$\eta_c = \exp\left(\frac{\ln(K_1) - \ln(K_2)}{n_2 - n_1} n_1 + \ln(K_1) + \frac{\ln(K_2) - \ln(K_1)}{n_2 - n_1}\right) \quad (7)$$

The whole procedure is performed respectively for the data in Figure 2a and for those in Figure 2b to obtain two different critical viscosity points for activation energy calculation. In this study, the values of n_1 and n_2 are set to 0.33 and 0.5.

3. Results and Discussion of the Preliminary Study

The protocol of the activation energy estimation process is summarized in Figure 4.

From the temperature data in Figure 2a (simulation S_1), we identify $K_1 = 9409.8 \text{ Pa}\cdot\text{s}^n$ and $K_2 = 4365.2 \text{ Pa}\cdot\text{s}^n$. The critical viscosity $[\eta_c]_{S_1}$ is 455.9 Pa.s for $\dot{\gamma}_c = 91.7 \text{ s}^{-1}$.

From the temperature data in Figure 2b (simulation S_2), we identify $K_1 = 7250.7 \text{ Pa}\cdot\text{s}^n$ and $K_2 = 3363.5 \text{ Pa}\cdot\text{s}^n$. The critical viscosity $[\eta_c]_{S_2}$ is 351.3 Pa.s for $\dot{\gamma}_c = 91.7 \text{ s}^{-1}$.

3.1. Activation Energy Estimation Result

The temperature fields are required to calculate the thermal dependence of viscosity. In a real experimental setup, it is difficult to know exactly the temperature field of the flow. The only reliable temperature measurements are the data in Figure 2. An average measured temperature can be calculated by following Equation (8).

$$\bar{T}_{obs} = \frac{\sum_{j=1}^{N_t} \sum_{i=2}^{N_{Th}} [T_{obs}]_{i,j}}{(N_{Th} - 1) N_t} \quad (8)$$

The average measured temperature $[\bar{T}_{obs}]_{S_1}$ in Figure 2a is 473.85 K. The average measured temperature $[\bar{T}_{obs}]_{S_2}$ in Figure 2b is 483.69 K. The activation energy can be estimated from Equation (9), which is in fact Equation (2) for observable quantities in a real experimental setup,

$$E_a = -R_g \frac{[\ln \eta_c]_{S_2} - [\ln \eta_c]_{S_1}}{[\bar{T}_{obs}]_{S_2} - [\bar{T}_{obs}]_{S_1}} [\bar{T}_{obs}]_{S_1} [\bar{T}_{obs}]_{S_2} \quad (9)$$

with $[\ln \eta_c]_{S_i}$ being $\ln \eta_c$ of the simulation S_i . The estimated activation energy is 50.5 kJ mol⁻¹, which is close to the targeted value at 50 kJ.mol⁻¹.

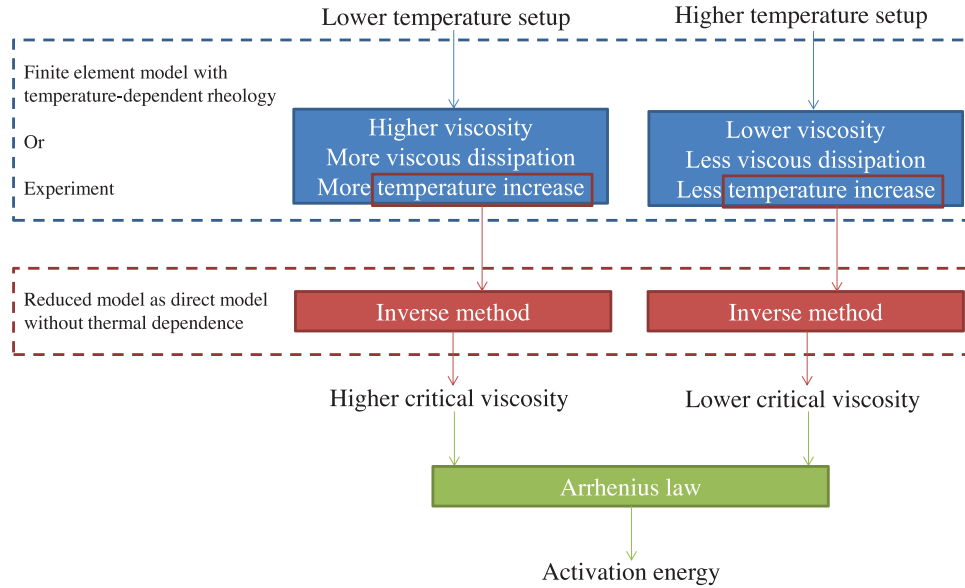


Figure 4. Protocol of the activation energy estimation process.

3.2. Estimation Error of the Inverse Method Process

The temperature field in the flow is not homogeneous. By considering the temperature variation, the finite element model uses Equation (2) to correct the viscosity in the flow. However, the reduced order model in the inverse method uses the same power-law viscosity expression (Equation (1)) for the entire flow domain without considering the thermal dependence and causes estimation errors. In other words, the inverse method can detect the thermal dependence when the temperature conditions pass from 473.15 K to 483.15 K. Nevertheless, the inverse method neglects the slight changes in viscosity caused by the temperature heterogeneity in the flow domain.

Between those two reference simulations in Figure 2, the temperature heterogeneity of simulation S_1 is greater, since higher viscosity at lower temperature causes more viscous dissipation. In order to study the error of using the same power-law viscosity expression over the flow domain without the thermal dependence, we re-run the first simulation without the thermal dependence (denoted simulation S'_1), the standard deviation between the temperature outputs of simulation S_1 and simulation S'_1 is 0.01 K. Compared to the temperature variations in Figure 2a, a standard deviation of 0.01 K is small.

The critical viscosity identified from the result of simulation S'_1 is 460.2 Pa.s for $\dot{\gamma}_c = 91.7 \text{ s}^{-1}$. The power law used in this study shows $\eta = 461.4 \text{ Pa.s}$ for $\dot{\gamma}_c = 91.7 \text{ s}^{-1}$ at 473.15 K. Without taking the thermal dependence into consideration, the inverse method is capable of delivering accurate result with slight errors due to the reduced order model's precision and the inverse method's numerical approximation. When the Arrhenius law (Equation (2)) is employed in the finite element model, the viscosity variation due to the heterogeneous temperature field in the flow does cause the inverse method to identify 455.9 Pa.s (from simulation S_1) instead of 460.2 Pa.s from (simulation S'_1). This difference is <1%.

Small changes in viscosity caused by temperature heterogeneity in the flow domain can be neglected, when the viscous heating is limited to a certain degree. Besides, for example, if all the viscosity terms in Equation (9) are multiplied by 101% (the same 1% error), the estimated activation energy remains the same.

4. Toward an Approach with Direct Temperature Measurement

The annular geometry has several interests. The virtual thermocouples of Figure 1 are insensitive to the set temperature on the outer surface of the duct thanks to the polymer flow barrier. When the virtual thermocouples are far enough from the outlet and insensitive to the outlet conditions, the only temperature conditions that influence the result are the inlet temperature and the initial temperature field.^[7] By considering that the inlet temperature is equal to the initial temperature (homogeneous initial temperature field), the temperature variations on the central axis, relative to the inlet/initial temperature, become sensitive only to the viscous dissipation, the velocity field of the flow and the thermal conductivities. In fact, the heat is generated by viscous dissipation within the flow and brought to the surface of the central axis by convection, which depends on the velocity field and the thermal conductivity of the melt.

Knowing that the viscosity variation due to the temperature heterogeneity in the flow can be neglected, one can consider using the average measured temperature to represent the whole temperature field of the flow. The entire flow domain therefore follows the same power-law expression (Equation (1)) with the same thermal-dependence correction (Equation (2)) as a function of the average measured temperature. In this case, the velocity field for a constant flowrate in a known annular geometry depends only on the pseudo-plasticity index $n^{[8,14]}$, i.e., $[\partial \ln(\eta) / \partial \ln(\dot{\gamma}) + 1]$. Thus, the velocity field does not depend on temperature, nor does the shear rate field.

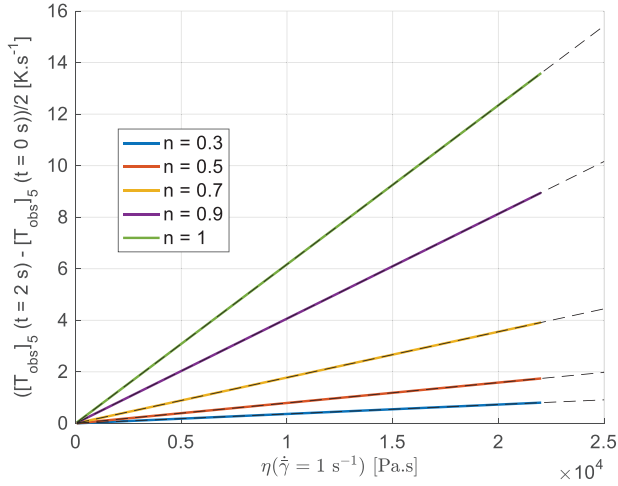


Figure 5. Linearity between the temperature increase rate and the viscosity at thermocouple 5.

So when we change the temperature conditions, for example from simulation S_1 to simulation S_2 , the difference is mainly in the viscous dissipation term $\eta \dot{\gamma}^2$ (precisely the viscosity η in the viscous dissipation term). The finite element model can be approximated to a system with a heat source proportional to the viscosity. The temperature increase rate $\partial[T_{obs,i}]/\partial t$ should be linear with respect to the power of the heat source and therefore linear with respect to the viscosity, which depends on the average measured temperature.

To confirm these hypotheses, massive simulation data is available from Figure 3 of the previous research.^[8] Those simulations consist of two-second injections with different power-law curves without taking into account the thermal dependence of viscosity.

If $\partial[T_{obs,i}]/\partial t$ is linear with respect to the viscosity, $\int_0^2 (\partial[T_{obs,i}]/\partial t) dt$ should be linear with respect to the viscosity. The temperature increase measured by thermocouple 5 at the end of the injection $([T_{obs}]_5(t=2\text{ s}) - [T_{obs}]_5(t=0\text{ s}))$ is divided by 2 seconds to assimilate the temperature increase rate $\partial[T_{obs,i}]/\partial t$, and presented in **Figure 5** as a function of the value of viscosity η when $\dot{\gamma} = 1\text{ s}^{-1}$.

Figure 5 shows that for each fixed value of n , the temperature increase rate is linear with respect to the viscosity. The dashed lines in Figure 5 are straight lines to visually confirm the linearity. As a result, the viscosity terms in Equation (9) can be replaced by temperature increase rates (equivalence (10)) of simulation S_1 and simulation S_2 ,

$$\eta_c \equiv A \left([T_{obs}]_{ij} - [T_{obs}]_{i,1} \right) \quad (10)$$

with $[T_{obs}]_{i,1}$ the initial temperature for thermocouple i and A a factor which has no influence in Equation (9). The activation energy can thus be estimated by directly using temperature measurements. There are different ways to carry out the estimation process. If we want to effectuate one estimation for each thermocouple at each recorded instant, we suggest to use $[T_{obs}]_{ij}$ to replace the average temperature terms in Equation (9) as well.

Table 1. Activation energy estimated by using measurements of each thermocouple at different instants.

Time [s]	Estimated activation energy E_a [kJ.mol ⁻¹]			
	$[T_{obs}]_2$	$[T_{obs}]_3$	$[T_{obs}]_4$	$[T_{obs}]_5$
0.5	50.4	50.2	49.9	49.6
1	50.8	50.7	50.5	50.2
1.5	51.2	51.2	51.1	50.8
2	51.5	51.7	51.6	51.4

Equation (9) becomes Equation (11),

$$E_a = -R_g \frac{\left[\ln \left([T_{obs}]_{ij} - [T_{obs}]_{i,1} \right) \right]_{S_2} - \left[\ln \left([T_{obs}]_{ij} - [T_{obs}]_{i,1} \right) \right]_{S_1}}{\left[[T_{obs}]_{ij} \right]_{S_2} - \left[[T_{obs}]_{ij} \right]_{S_1}} \times \left[[T_{obs}]_{ij} \right]_{S_1} \left[[T_{obs}]_{ij} \right]_{S_2} \quad (11)$$

where $\left[\ln \left([T_{obs}]_{ij} - [T_{obs}]_{i,1} \right) \right]_{S_k}$ is the natural logarithm of the temperature increase relative to the initial temperature for thermocouple i at instant j in simulation S_k , and $\left[[T_{obs}]_{ij} \right]_{S_k}$ is the absolute temperature for thermocouple i at instant j in simulation S_k . The activation energy estimation result for each thermocouple at four different recorded instants is shown in **Table 1**.

Most of the results in Table 1 are close to the targeted value of the activation energy at 50 kJ.mol⁻¹, despite those hypotheses that we use in this approach. Over time, the temperature field in the flow becomes more and more heterogeneous due to the viscous dissipation; the hypothesis neglecting the viscosity variation due to the temperature heterogeneity in the flow induces more and more estimation errors.

5. Toward an Approach with the Time-Temperature Superposition Principle^[1]

The simple coupling of Equation (1) and Equation (2) in the finite element model is used to perform analyses for the development of the approach so far. However, this coupling is far from being realistic to represent the rheological behavior of a polymer in a large range of shear rate. In fact, for a material with Newtonian behavior in the low shear rate range and shear thinning behavior in the high shear rate range, the ratio $\eta(T)/\eta(T_0)$ depends on the shear rate.^[15] For example, the Cross law (Equation (12))^[16] is one of the rheological models which better describe the behavior of a polymer,

$$\eta = \frac{\eta_0 a_{T/T_0}}{1 + \left(\frac{\eta_0 a_{T/T_0}}{\tau^*} \dot{\gamma} \right)^{1-n}} \quad (12)$$

with η_0 the zero shear rate viscosity at temperature T_0 , τ^* the critical stress level at the transition to shear thinning regime and

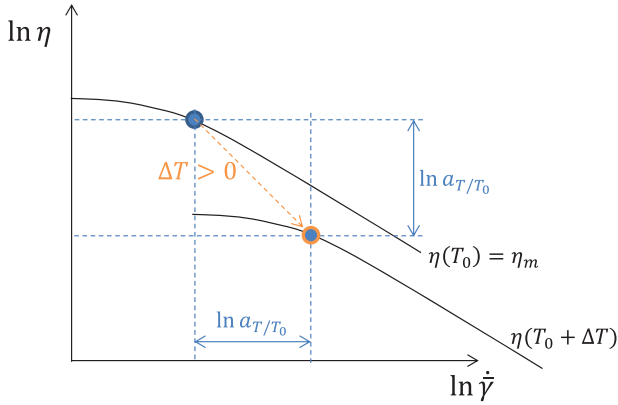


Figure 6. Temperature dependence of the Cross law (Equation (12)).

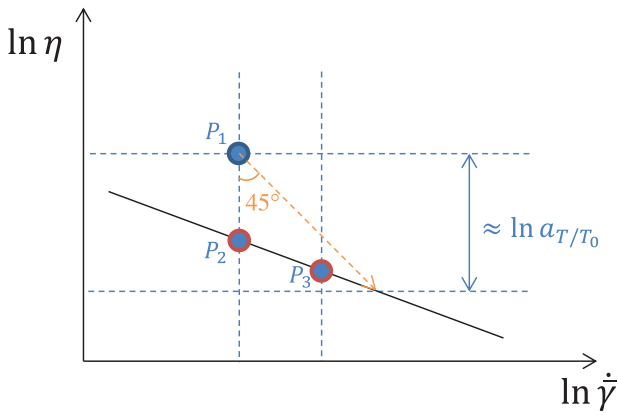


Figure 7. Estimation process of a_{T/T_0} .

a_{T/T_0} the thermal translation factor following the Arrhenius law (Equation (13)).^[3]

$$a_{T/T_0} = \exp \left[\frac{E_a}{R_g} \left(\frac{1}{T} - \frac{1}{T_0} \right) \right] \quad (13)$$

A master curve, with $[\eta_m = \eta/a_{T/T_0}]$ as a function of $[\dot{\gamma}_m = a_{T/T_0}\dot{\gamma}]$, can be drawn from Cross-law curves (Equation (12)) at different temperatures. This is called the time-temperature superposition principle.^[1] That is to say that, in this case, the thermal dependence (a_{T/T_0} from Equation (13)) shifts the viscosity curves vertically and horizontally (away from the master curve) on a logarithmic scale:

- $\ln(\eta_m a_{T/T_0}) = \ln \eta_m + \ln a_{T/T_0}$;
- $\ln(\dot{\gamma}_m / a_{T/T_0}) = \ln \dot{\gamma}_m - \ln a_{T/T_0}$.

as shown in **Figure 6** (with $\ln a_{T/T_0} < 0$, temperature increase).

Therefore, the activation energy estimation from critical viscosity values at the same critical shear rate (i.e., using Equation (9)) will induce errors, especially at the shear thinning regime, as shown in Figure 6. A modification must be made to the estimation process by taking the principle of time-temperature superposition into consideration.

An estimation process of a_{T/T_0} is illustrated in **Figure 7**. A critical viscosity point P_1 is first identified from experimental data.

Table 2. Identified critical points P_1, P_2 and P_3 .

	η_c [Pa.s]	$\dot{\gamma}_c$ [s^{-1}]	Flowrate [$cm^3 \cdot s^{-1}$]	Temperature conditions [K]
P_1	463.7	91.7	56.5	473.15
P_2	413.3	91.7	56.5	483.15
P_3	369.2	112.4	70.7	483.15

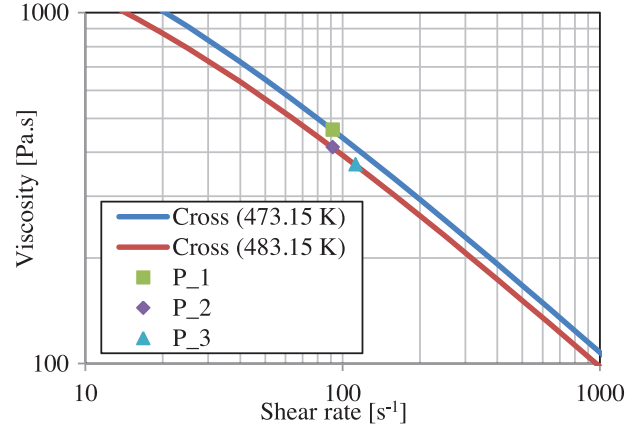


Figure 8. Identified critical points P_1, P_2 and P_3 with Cross law curves at 473.15 and 483.15 K.

The experimental temperature setup is then changed to obtain another critical viscosity point P_2 . With the same experimental temperature setup of critical point P_2 , the third critical viscosity point P_3 can be obtained at a different flowrate. If we consider that P_2 and P_3 are identified under the same temperature condition, these two critical points can be used to draw an approximated viscosity line (local power-law curve). Starting from P_1 , following the 45° direction, arriving to the approximated viscosity line, this distance can be assimilated to $\sqrt{2} \ln a_{T/T_0}$ (orange dashed arrow in Figure 7). When a_{T/T_0} is known, E_a can be calculated from Equation (13).

In the finite element model, the rheological law is replaced by Equation (12) with $\eta_0 = 3192.75$ Pa.s, $\tau^* = 19996.2$ Pa and $n = 0.3387$. In Equation (13), $E_a = 50$ kJ.mol⁻¹ and $T_0 = 473.15$ K. Three virtual two-second injections are simulated with the finite element model for:

- temperature conditions at 473.15 K, flowrate at 56.5 $cm^3 \cdot s^{-1}$ to identify critical point P_1 ;
- temperature conditions at 483.15 K, flowrate at 56.5 $cm^3 \cdot s^{-1}$ to identify critical point P_2 ;
- temperature conditions at 483.15 K, flowrate at 70.7 $cm^3 \cdot s^{-1}$ to identify critical point P_3 .

The result of the critical point identification is shown in **Table 2**. For the same injection duration, the variation of critical shear rate is nearly linear with respect to the variation of flowrate, which is consistent with the observation in the previous research.^[8]

These critical points are plotted in **Figure 8**. Two Cross law curves at 473.15 and 483.15 K are also presented.

In Figure 8, P_1 is on the Cross law curve at 473.15 K; P_2 and P_3 is on the Cross law curve at 483.15 K. The precision of the

inverse method is demonstrated here. According to the analysis in Figure 7 and the identified critical points, we can calculate Equation (14) and obtain $\ln a_{T/T_0} = -0.257$.

$$\ln a_{T/T_0} \approx \frac{[\ln \eta_c]_{P_2} - [\ln \eta_c]_{P_1}}{1 + \frac{[\ln \eta_c]_{P_2} - [\ln \eta_c]_{P_3}}{[\ln \dot{\gamma}_c]_{P_2} - [\ln \dot{\gamma}_c]_{P_3}}} \quad (14)$$

In Equation (14), $[\ln \eta_c]_{P_i}$ and $[\ln \dot{\gamma}_c]_{P_i}$ are $\ln \eta_c$ and $\ln \dot{\gamma}_c$ of critical point P_i . $[\ln \eta_c]_{P_2} - [\ln \eta_c]_{P_3} / ([\ln \dot{\gamma}_c]_{P_2} - [\ln \dot{\gamma}_c]_{P_3})$ represents the slope (on a logarithmic scale) calculated from P_2 and P_3 . If P_2 and P_3 are considered as two points on a power-law curve, the slope is $(n - 1)$. When n tends to zero, the slope tends to -1.

The melt temperatures are then necessary to drive the activation energy estimation process to the end. The set temperature can be poorly respected in a real experiment. The only reliable temperature information comes from measurements. The average measured temperature in the first virtual experiment (P_1) is 473.96 K. The temperature signals of the second and the third virtual experiments (P_2 and P_3) are all used to calculate an average value : 483.98 K. The activation energy can be calculated from Equation (15),

$$E_a = \frac{1}{1 + \frac{[\ln \eta_c]_{P_2} - [\ln \eta_c]_{P_3}}{[\ln \dot{\gamma}_c]_{P_2} - [\ln \dot{\gamma}_c]_{P_3}}} \times \left[-R_g \frac{[\ln \eta_c]_{P_2} - [\ln \eta_c]_{P_1}}{[\bar{T}_{obs}]_{P_2 \& P_3} - [\bar{T}_{obs}]_{P_1}} [\bar{T}_{obs}]_{P_1} [\bar{T}_{obs}]_{P_2 \& P_3} \right] \quad (15)$$

with $[\bar{T}_{obs}]_{P_1}$ the average measured temperature in the first virtual experiment (P_1) and $[\bar{T}_{obs}]_{P_2 \& P_3}$ the average measured temperature in the second and the third virtual experiments (P_2 and P_3).

Using Equation (15), we can calculate $E_a = 48.9 \text{ kJ mol}^{-1}$. The result is slightly different from the targeted value at 50 kJ mol^{-1} due to the approximation in Figure 7. In fact, even if P_2 and P_3 are really on a Cross-law curve for the same temperature, the slope of the curve on the right side of P_3 (Figure 8) is more negative than the slope calculated from $[\ln \eta_c]_{P_2} - [\ln \eta_c]_{P_3} / ([\ln \dot{\gamma}_c]_{P_2} - [\ln \dot{\gamma}_c]_{P_3})$. The result is thus underestimated because of this variation of the slope.

In the previous section, an approach is proposed to use only direct temperature measurements for activation energy estimation. It is difficult to proceed in the same way for the estimation process presented in this section. Relation (10) is only valid for simulations/experiments carried out with the same flowrate. Indeed, the viscous dissipation power is not linear with respect to the flowrate. Moreover, the change in the flowrate will modify the convective exchange between the central axis and the polymer flow. Consequently, P_3 obtained with another flowrate is the main hurdle here. One possible solution is to calculate the slope $[\ln \eta_c]_{P_2} - [\ln \eta_c]_{P_3} / ([\ln \dot{\gamma}_c]_{P_2} - [\ln \dot{\gamma}_c]_{P_3})$ in Equation (14) in another way to avoid using P_3 . For example, the value of $\partial \ln(\eta) / \partial \ln(\dot{\gamma})$ can be identified by a convection method.^[14]

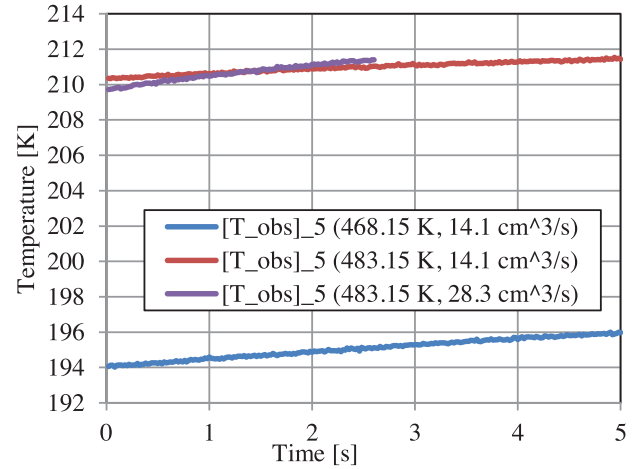


Figure 9. Experimental measurements of thermocouple five on the polystyrene (ATOFINA LACQRENE 1540) air shot tests for different set temperature and flowrate configurations.

6. Experimental Test of the Approaches

The TRAC is equipped with type K thermocouples. During the calibration test, the standard deviation among thermocouples 2 to 5 is $<0.06 \text{ K}$. The standard deviation of the measurement noise of each thermocouple is 0.03 K .

During a real experiment, polystyrene melt (ATOFINA LACQRENE 1540) is injected through the TRAC.^[7] Three air shots (without mold) are performed:

- Air shot I_1 with a set temperature at 468.15 K and a flowrate at $14.1 \text{ cm}^3 \text{ s}^{-1}$;
- Air shot I_2 with a set temperature at 483.15 K and a flowrate at $14.1 \text{ cm}^3 \text{ s}^{-1}$;
- Air shot I_3 with a set temperature at 483.15 K and a flowrate at $28.3 \text{ cm}^3 \text{ s}^{-1}$.

The temperature variation is measured for each air shot. Only the measurements of thermocouple five are presented in Figure 9 for readability.

The duration of the third air shot is shorter because the flowrate is doubled, and the injection volume remains constant. The temperature in the third air shot increases more rapidly compared to that of the second air shot with a lower flowrate.

A quick analysis of the thermal dependence of viscosity is effected with Equation (11) and the measurement data of air shots I_1 and I_2 . The estimated activation energy is presented in Figure 10. As in Table 1, an estimated activation energy is given for each thermocouple $i \in \{2; 5\}$ at each instant. An average curve of estimates of those four thermocouples is also presented in Figure 10.

Some estimates are negative due to measurement noise, especially at the beginning of the air shots where the temperature increases due to the viscous dissipation remains small. These negative estimates are not presented in Figure 10. However, the estimation uncertainty at the start of the air shots is still higher compared to that after 2 seconds of air shot. The estimated activation energy is close to $50\text{--}140 \text{ kJ mol}^{-1}$ from 4 to 5 s in Figure 10. The variance between the estimated values for different

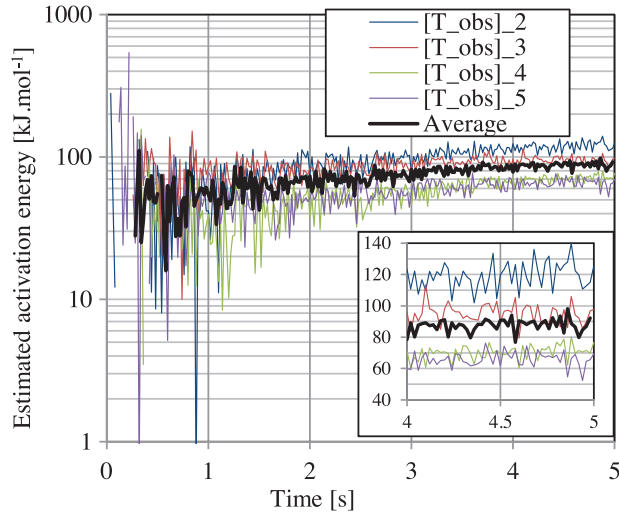


Figure 10. Activation energy estimated for each thermocouple at each instant by applying Equation (11) to the measurement data of air shots I_1 and I_2 .

Table 3. Identified critical points for air shot experiments.

Air shot	η_c [Pa.s]	$\dot{\gamma}_c$ [s^{-1}]	Flowrate [$cm^3.s^{-1}$]	Temperature conditions [K]	\bar{T}_{obs} [K]
I_1	2950.7	24.5	14.1	468.15	468.34
I_2	1465.5	24.5	14.1	483.15	484.19
I_3	1193.5	48.2	28.3	483.15	483.89

thermocouples in a real experiment is much higher compared to the numerical result in Table 1.

We would like to mention that for injections < 2 s, as long as the temperature increase is large enough compared to the measurement noise/fluctuation, the estimation uncertainty can be less than what is shown in Figure 10 for the first 2 s. To obtain a higher temperature increase rate, the flowrate can be set to a higher value.

This approach employing only direct temperature measurements can be useful for temperature dependent flow models over a limited range of shear rates, where the flow viscosity can be considered to follow a power law. In other words, it can be performed at the Newtonian regime, the pseudo-plastic regime, or the transition region between these two regimes, as long as the dominant part of the viscosity curve can be approximated by a power law. The range of validity depends on the curvature of the dominant part of the viscosity law. Ideally, this approach should be performed at a high shear rate regime. Nevertheless, the fidelity of the measurement environment to the hypotheses of the numerical/analytical model should be improved for a reliable application of the approach.

To apply the other approach with the time–temperature superposition principle, the critical points are identified by inverse method and presented in Table 3. The average measured temperature \bar{T}_{obs} is also shown in Table 3.

With the information in Table 3, Equation (14) can be used to obtain the value of $\ln a_{T/T_0}$, which is -1. Consequently, $E_a = R_g \ln a_{T/T_0} / [1/468.34 - 2/(484.19 + 483.89)] = 120.7 \text{ kJ mol}^{-1}$.

(The temperature signals from the second and third air shots are put together to calculate an average temperature.) The differential dE_a in this case can be calculated by taking the partial derivatives of Equation (15) and written as Equation (16) for error estimation,

$$dE_a = 7940.4d[\bar{T}_{obs}]_{I_1} - 7433.5d[\bar{T}_{obs}]_{I_2 \& I_3} + 58.4d[\eta_c]_{I_1} + 57.6d[\eta_c]_{I_2} - 215.2d[\eta_c]_{I_3} \quad (16)$$

with $[\eta_c]_{I_i}$ the critical viscosity of air shot I_i , $[\bar{T}_{obs}]_{I_1}$ the average measured temperature in air shot I_1 and $[\bar{T}_{obs}]_{I_2 \& I_3}$ the average measured temperature in air shot I_2 and I_3 .

We would like to mention that if we apply Equation (9) with the critical points of air shots I_1 and I_2 , the estimated activation energy is 83.2 kJ mol^{-1} , which is consistent with the average curve in Figure 10, but lower than the estimation of the approach with the time–temperature superposition principle. Equation (14) and Equation (15) show that this difference is related to the local slope of the viscosity curve constructed from the critical points of air shots I_2 and I_3 . Equation (15) is in fact equivalent to Equation (9) with a factor calculated from the local slope. When the local slope tends to zero, the approach corresponding to Equation (15) converges to the approach corresponding to Equation (9). The slope calculated from the critical points of air shots I_2 and I_3 is -0.304 according to the data in Table 3. If we multiply the result of 83.2 kJ mol^{-1} by the factor $[1/(1-0.304)]$: $83.2/(1 - 0.304) = 118.9 \text{ kJ mol}^{-1}$, the value is actually close to $120.7 \text{ kJ mol}^{-1}$.

The value of 83.2 kJ mol^{-1} should be used with Equation (1) and Equation (2) to effectively model the flow behavior over a limited shear rate range. This value does not necessarily represent the actual activation energy, unless it is estimated at low shear rates where the local slope of the viscosity curve approaches zero.^[15]

The value of $120.7 \text{ kJ mol}^{-1}$ should be used with Equation (12) and Equation (13) for modeling over a large shear rate range. This value represents better the actual activation energy.

7. Conclusion

Numerical and experimental studies are carried out with an annular measuring device^[7] (TRAC : Thermo-Rheo Annular Cell), which can provide robust temperature measurements of a polymer flow. The temperature variation due to the viscous dissipation in the flow can be used to identify critical viscosity points by inverse method. Critical viscosity points identified at different temperatures (the thermal dependence of viscosity) can be employed for the estimation of activation energy. The preliminary numerical study first demonstrates the mechanism of exploiting the phenomenon of viscous dissipation for viscosity identification at different temperatures to estimate the activation energy.

By considering the thermal characteristics of the annular flow for a given flowrate, a direct correlation can be established between temperature variation due to the viscous dissipation and the viscosity. Temperature measurements can be used directly to calculate activation energies without the need for inverse method. However, this approach is based on power-law type

viscosity curves with the Arrhenius law acting on the viscosity values. The estimated activation energy value can be criticized depending on the shear rate regime.^[15] Still, the activation energy estimated in this way is sufficient to model the thermal dependence of a simple power-law type viscosity at high shear rate regime.

Another approach is proposed with the principle of time-temperature superposition. The flowrate and the flow temperature need to be modified to identify three critical viscosity points to estimate the activation energy. The activation energy estimated in this way works for a large shear rate range with more complex viscosity laws, such as the Cross law.

Finally, the experiment demonstrates the application of the proposed approaches on real material. The variance of the estimated results is influenced by the difference between the actual measurement environment and the hypotheses of the numerical/analytical model.

Acknowledgements

This study was supported by the French Ministry of Higher Education, Research and Innovation and held in IUT Nantes.

Conflict of Interest

The authors declare no conflict of interest.

Data Availability Statement

The data that support the findings of this study are available from the corresponding author upon reasonable request.

Keywords

annular flow, polymers, temperature, thermal dependence, viscosity

Received: March 2, 2023

Revised: May 22, 2023

Published online: June 4, 2023

-
- [1] J. F. Agassant, P. Avenas, P. J. Carreau, B. Vergnes, M. Vincent, *Polymer Processing: Principles and Modeling*, Carl Hanser Verlag GmbH Co KG, Munich, Germany **2017**.
 - [2] S. Glasstone, K. J. Laidler, H. Eyring, *The Theory of Rate Processes; the Kinetics of Chemical Reactions, Viscosity, Diffusion and Electrochemical Phenomena*, McGraw-Hill Book Company, New York, USA **1941**.
 - [3] S. Arrhenius, *Z. Für Phys. Chem.* **1889**, *4U*, 96.
 - [4] B. Rabinowitsch, *Z. Für Phys. Chem.* **1929**, *145*, 1.
 - [5] W. P. Cox, E. H. Merz, *J. Polym. Sci.* **1958**, *28*, 619.
 - [6] C. Abeykoon, *Meas. Sens.* **2022**, *22*, 100381.
 - [7] Q. Lin, N. Allanic, P. Mousseau, Y. Madec, G. Beau, R. Deterre, *Polym. Eng. Sci.* **2022**, *62*, 3994.
 - [8] Q. Lin, N. Allanic, R. Deterre, P. Mousseau, M. Girault, *Int. J. Heat Mass Transf.* **2022**, *182*, 121988.
 - [9] Q. Lin, N. Allanic, P. Mousseau, M. Girault, R. Deterre, *Int. J. Heat Mass Transf.* **2023**, *206*, 123954.
 - [10] W. Ostwald, *Kolloid Z.* **1925**, *36*, 99.
 - [11] A. de Waele, *J. Oil Colour Chem. Assoc.* **1923**, *6*, 33.
 - [12] M. Girault, Q. Lin, N. Allanic, P. Mousseau, *Int. J. Heat Mass Transf.* **2023**, *203*, 123692.
 - [13] R. Deterre, P. Mousseau, A. Sarda, *Injection Des Polymères: Simulation, Optimisation et Conception*, Tec & Doc Lavoisier, France, **2003**.
 - [14] Q. Lin, N. Allanic, M. Girault, R. Deterre, P. Mousseau, *Key Eng. Mater.* **2022**, *926*, 1914.
 - [15] G. M. Bartenev, *Polym. Sci. U.S.S.R.* **1964**, *6*, 383.
 - [16] M. M. Cross, *J. Colloid Sci.* **1965**, *20*, 417.